Microelectrochemical Investigation of the Effect of Cathodic Polarisation on the Corrosion Resistance of 304L Stainless Steel in a 1 M NaCl Solution

Farzin Arjmand and Annemie Adriaens[*]

Department of Analytical Chemistry, Ghent University, Krijgslaan 281-S12, 9000 Ghent, Belgium
[*]E-mail: annemie.adriaens@ugent.be

304L stainless steel was cathodically polarised in a 1 M sodium chloride solution using a microcapillary electrochemical droplet cell. During the cathodic polarisation the produced hydrogen atoms penetrate into the sample and accumulate at sites of the steel surface. We observed that the pitting potential (E_{pit}), the anodic current density (I_{corr}) and the corrosion potential (E_{corr}) of the polarised steel are strongly influenced by the applied cathodic potential and therefore by the amount of charged hydrogen atoms which penetrate into the sample. Local electrochemical impedance spectroscopy (LEIS) using different applied cathodic potentials shows lower corrosion resistance for cathodically polarised steel and reveals a different behaviour on a microscale level.

1. INTRODUCTION

The evolution of gas bubbles is a well-known phenomenon during the formation of corrosion pits for materials such as aluminium and iron [1]. Pickering and Frankenthal [2] have identified the gas as hydrogen in aqueous solutions. During the corrosion process, hydrogen reduction and metal dissolution occur simultaneously in the metal-electrolyte interface. Part of charged hydrogen can absorb on the metal surface and diffuses into the corroding area [2-5] and the rest of the hydrogen forms gas and/or water molecules and escapes. The generated hydrogen atoms, which penetrate into the metal, locally break down the existing oxide film and form small pinholes/sites. These pits act as preferential sites during the anodic dissolution of the metal [1].

Although there is still serious debate on the role of hydrogen in pit corrosion and blister formation of metals, it is clear that hydrogen increases the corrosion rate [6], promotes the anodic dissolution [7], decreases the stability of the passive layer [8], increases the pitting susceptibility [9] and also increases the passive current density of iron-based alloys [10]. It also has been shown that there is an interaction between hydrogen and chloride ions during the corrosion process in chloride containing media [11].

In the case of prior potentiostatic polarisation the hydrogen charging procedure occurs with a higher intensity and therefore the cathodic corrosion forms micro pits on the metal surface [12-22]. Despite all the previous performed studies to date, the synergistic effect of hydrogen and the anodic dissolution on a micro scale level remain largely unknown. Therefore in this work, we investigate the effect of the hydrogen evolution during a micro potentiostatic polarisation on the corrosion resistance of the steel. Here the use of the microcapillary technique has a key role. It is capable of performing electrochemical measurements on a defined point of the sample and at the same time it has shown its high ability in surface analysis for the study of various metals and alloys such as the microelectrochemical behaviour of copper, 316L steel and aluminium or the investigation of aluminium–steel friction welds [23-29]. In our previous work, for instance, we showed that localisation of the measurement area using a microcapillary cell has significant effects on the electrochemical response of metals and alloys during their corrosion process, especially in the case of electrochemical impedance spectroscopy [30].

2. EXPERIMENTAL

2.1. Chemicals

A 1 M sodium chloride solution was prepared using analytical grade NaCl powder (Fluka). In addition a mixture of 1.5:1 ratio HNO_3/H_2O was prepared to etch the sample.

2.2. Specimen and surface preparation

A 304L stainless steel coupon with the following chemical composition (wt. %): Cr: 17.65, Ni: 8.59, Mn: 1.75, Si: 0.41, C: 0.017, P: 0.032 and S: 0.005 was used in this study. The sample (diameter of 12.5 mm and thickness of 2 mm) was mechanically ground with silicon carbide paper down to 600 grit, and then polished with a polishing cloth (MicroCloth, Buehler) using alumina powder (< 1 μm). The sample was washed with distilled water and then rinsed ultrasonically in ethanol for 5 minutes.

Observation of the steel microstructure became possible after a surface etching procedure. Etching was done by immersing a polished steel coupon in a 1.5 : 1 mixture of HNO_3/H_2O for up to 80 s [31]. An optical image of the steel coupon after etching is shown in Figure 1. The mean grain size of the steel was estimated using the linear intercept method. The main idea of this method is counting the number of grains intercepted by one or more straight lines sufficiently long enough to yield at least 50 intercepts [32]. The mean grain size of the steel used in this work is about 19.26 μm. The latter was

obtained after three linear intercept measurements on three microscopic images of different areas of the sample.
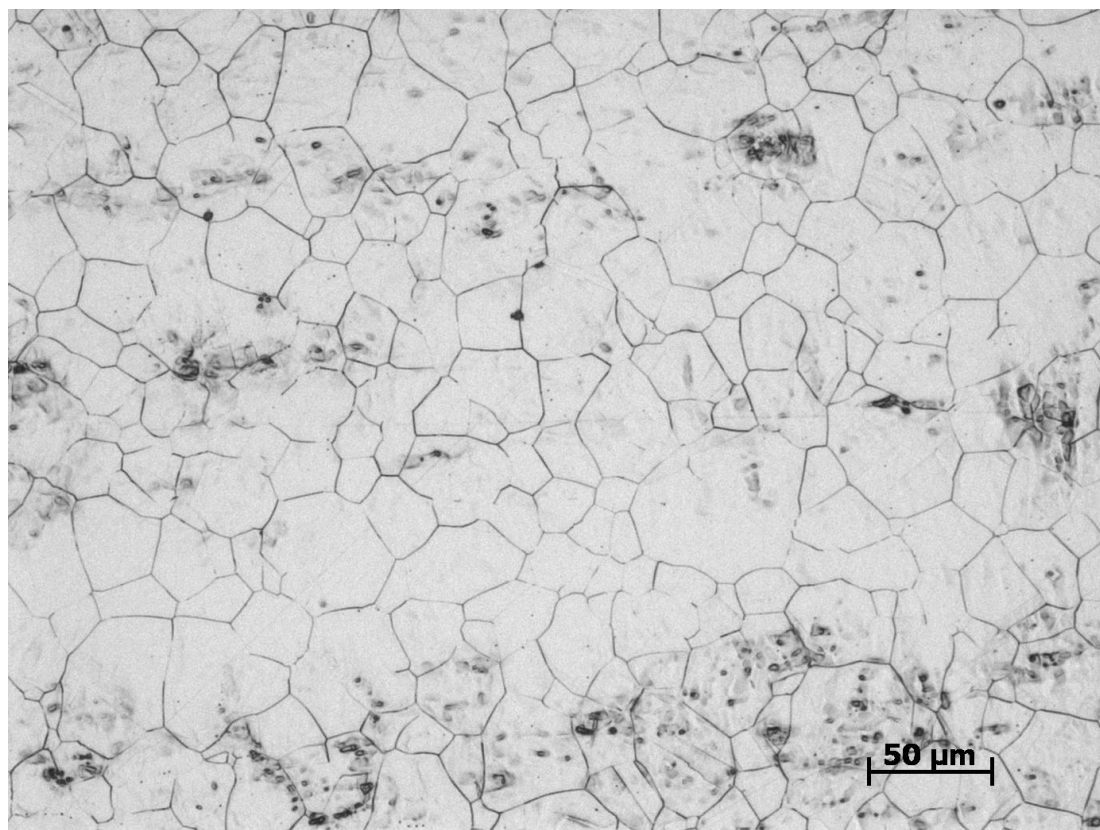

Figure 1. Optical image of the microstructure of the etched 304L stainless steel sample .

2.3. Preparation of the microcapillary with silicone gasket

2 mL glass Pasteur pipettes were used to make the microcapillaries. The pipettes were heated till the glass melting point and pulled carefully, resulting in appropriate tip diameters. The tip surface of the prepared capillaries was polished using first 600 and then 1200 grit silicon carbide (SiC) papers. A silicone gasket was attached to the polished tips in order to prevent leaking of the electrolyte. The gasket was prepared by dipping the capillaries into silicone rubber, after which a stream of nitrogen was flushed through the microcapillary to keep the tip of the capillaries open without destroying the gasket. An optical microscope was used to monitor the procedure. By repeating this procedure for 2 or 3 times, thin layers of silicone were applied onto the tip of the capillaries.

One of the limitations with microcapillaries, especially at high cathodic potentials or low scan rates, is that reaction products and gas bubbles can block the capillary channel during the measurements. This can be easily detected by a rapid dropping in the oxidation or reduction current. This instability in the electrochemical response usually is observed at the beginning of the measurement and then decreases when the first generated gas bubbles escape. According to our experience, one can avoid this problem by using a higher scan rate. This also has been reported before

by other authors [28-30, 33]. In addition, compared to other microcapillary work, where one uses extremely small capillary diameters (till 1 μm), here we make use of a larger diameter (200 μm) to avoid some technical problems mentioned-above and also overcome other limitations of the microcapillary technique such as ohmic drop and the need of using a high resolution potentiostat.

2.4. Electrochemical set-up

A schematic design of the homemade microcapillary electrochemical cell used in this work has been shown in in our previous work [30]. The setup involves a thin platinum wire as counter electrode, a saturated Ag/AgCl reference electrode and the sealed microcapillary attached to an Autolab Eco Chemie potentiostat (PGSTAT 10). The main idea of the microcapillary system is the miniaturisation of the working electrode surface area, which results in more detailed information regarding pit corrosion. In this setup the sealed tip of the microcapillary filled with 1 M sodium chloride solution only touches a small part of the sample and makes the working electrode very small (micro scale). It is clear that one can easily calculate the wetted surface area under the microcapillary (working electrode) using the microcapillary tip diameter (in this work: tip diameter ~ 200 μm/ wetted area ~ 0.03 mm^2). Although the amount of the electrolyte inside the microcapillary tip is small, the microcapillary cell contains a bulk electrolyte in which the reference and the counter electrodes are immersed. In fact the counter electrode is placed 3 to 5 cm above the tip. Therefore the oxidation or reduction processes, which occur in the electrolyte-surface interface do not affect the surface area of the counter electrode.

2.5. Electrochemical measurements

The potentiostatic polarisation was performed at different potentials (-1 V, -1.3 V, -1.5 V, -1.7 V and -1.9 V) each with a duration time of 600 s. Tafel plots of the steel sample were recorded before and after each cathodic polarisation in the potential range of -1.5 and 1.3 V (vs. Ag/AgCl) and a scan rate of 10 mV/s. The latter allowed us to determine the corrosion potentials, corrosion currents and also the pitting potentials of the stainless steel under the different conditions. In between the potential polarisation at a specific voltage, followed by the linear sweep voltammetry as described above, the microcapillary was moved to another spot of the sample for a new set of measurements at a different potential.

Localised electrochemical impedance spectroscopy measurements (LEIS) of the steel sample were carried out in a frequency range of 50 kHz to 0.1 Hz (amplitude of 25 mV at open circuit potential). The Nyquist plots were recorded before and after the potentiostatic polarisation of the wetted surface. Also here, after each cathodic polarisation, Nyquist plots were recorded on the same spot without (re)moving the sample. Each series of the measurements was performed on one steel coupon after one surface preparation procedure in two small surface areas of about 4 × 4 mm next to each other for both the Tafel plot measurements and the LEIS experiments. In order to test the reproducibility of the measurements the experiments were also repeated on two other coupons under the same conditions.

2.6. XPS measurements

The surface analysis of the measured area after the electrochemical measurements was performed by X-ray photoelectron spectroscopy (S-probe monochromatized XPS spectrometer) with a voltage and power of the source of respectively 10 KV and 200 W.

3. RESULTS AND DISCUSSION
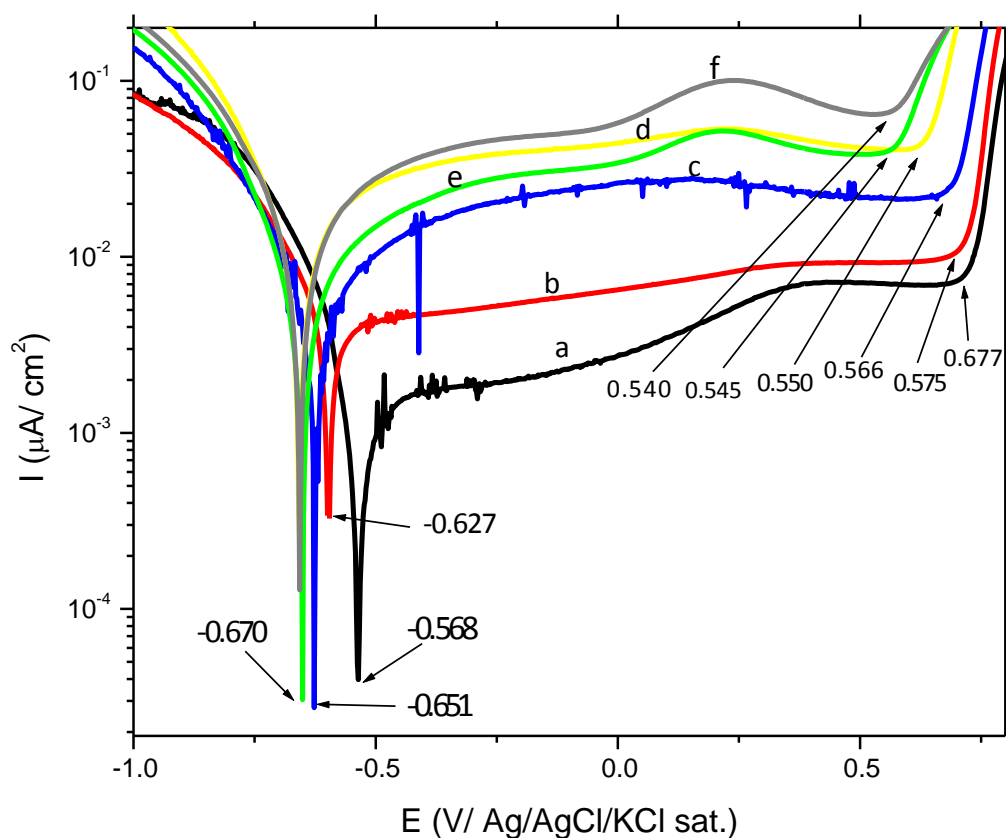
3.1. Potentiostatic and potentiodynamic polarisation

Figure 2. Variations of the anodic current density, E_{corr} and E_{pit} of steel (a) before and after 600 s of potentiostatic polarisation at five different potentials (b) -1 V, (c) -1.3 V, (d) -1.5 V, (e) -1.7 V and (f) -1.9 V in a 1 M sodium chloride solution. Tip diameter of the microcapillary is ca. 200 μm.

Figure 2 shows the variation of the corrosion potential (E_{corr}), the anodic current density (I_{corr}) and the pitting potential (E_{pit}) of the steel sample in the 1 M sodium chloride solution before and after potentiostatic polarisation. The corrosion potential of steel after the cathodic polarisation decreases continuously as the polarisation potential increases. The potential for the non-polarised sample is around -0.568 V (vs. Ag/AgCl) and this decreases to -0.627 V (vs. Ag/AgCl) after the polarisation of -1 V during 600 s. By increasing the cathodic polarisation to -1.3 V, the corrosion potential of the

sample decreases to -0.651 V (vs. Ag/AgCl). Finally after polarising the sample at -1.5 V and -1.9 V, the corrosion potential of steel decreases further to -0.670 V (vs. Ag/AgCl).

Figure 2 also demonstrates that the pit initiation of the non-polarised steel sample appears at 0.677 V (vs. Ag/AgCl) while after the potentiostatic polarisation of -1 V, the pit nucleation starts at more negative potentials (0.575 V vs. Ag/AgCl) and then continuously drops till 0.540 V (vs. Ag/AgCl) as the cathodic polarisation potential increases.

Another effect of the cathodic polarisation appears at the anodic part of the Tafel plots in Figure 2 where the anodic current density and therefore the corrosion current (I_{corr}) increases when applying higher cathodic potentials. The calculated (I_{corr}) for the non-polarised steel increases after the potentiostatic polarisation with increasing the applied cathodic potential.

Overall, Figure 2 clearly shows that the pitting potential, the corrosion potential and the corrosion current and in general the corrosion resistance depend on the applied cathodic potential which cathodically corrodes metals/ alloys. This current and the potential shift and its amount are attributed to the charged hydrogen atoms, which absorb on the passive layer [1].

It has been proven that passive layers on ferrous alloys such as stainless steel act as semiconductor films [34-35]. The absorbed hydrogen can be reduced and therefore effect on the semiconductive properties of steel passive layer and form a new surface nanostructure including micro pits. Moreover, during the potentiodynamic polarisation in sodium chloride containing solutions chloride ions can attack to these pits/ sites and cause anodic dissolution of the surface.

The chemical composition of the corroded area after 600 s potentiostatic polarisation at -1.3 V and after a potentiodynamic polarisation was studied by XPS (Figure 3). The spectra show only steel elements with the highest concentration (here Fe, Cr). Low intensity peaks of Na and Cl also were detected which are not mentioned in this figure. According to these results the expected composition of the corroded area of the steel are mainly Fe_2O_3 and Cr_2O_3 plus small amounts of $FeCl_3$ and $CrCl_3$.
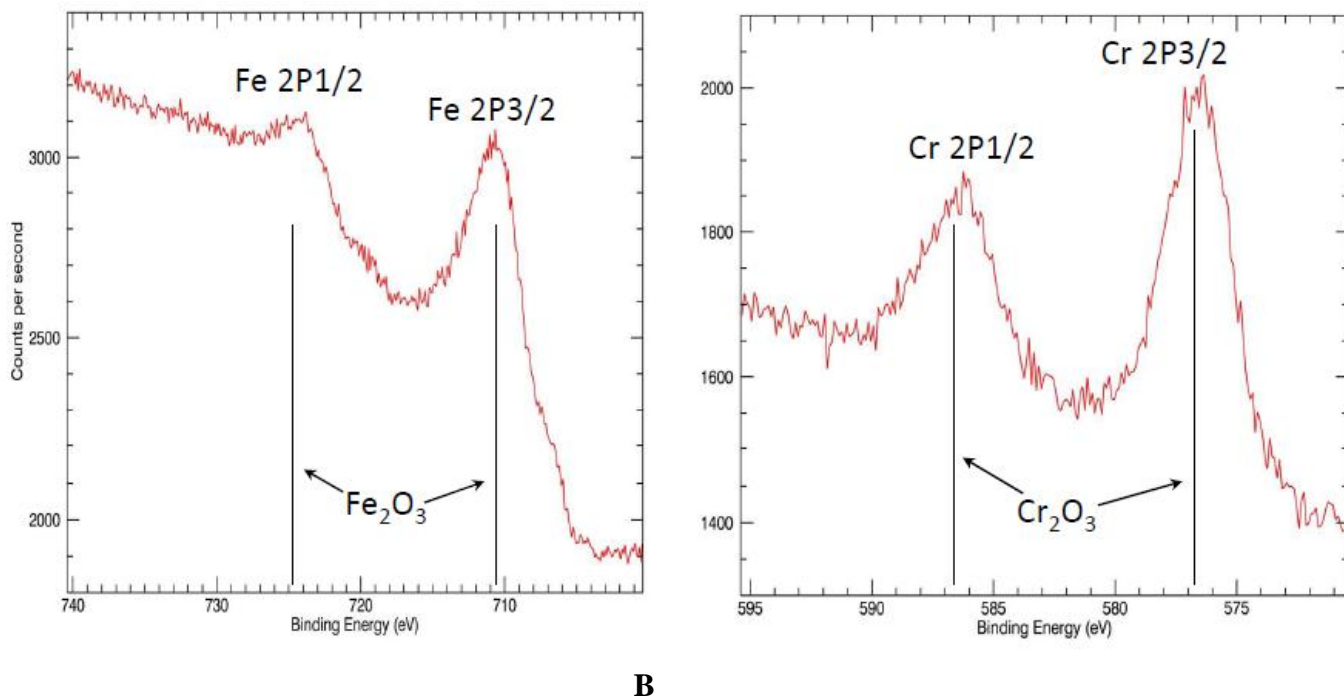

A

B
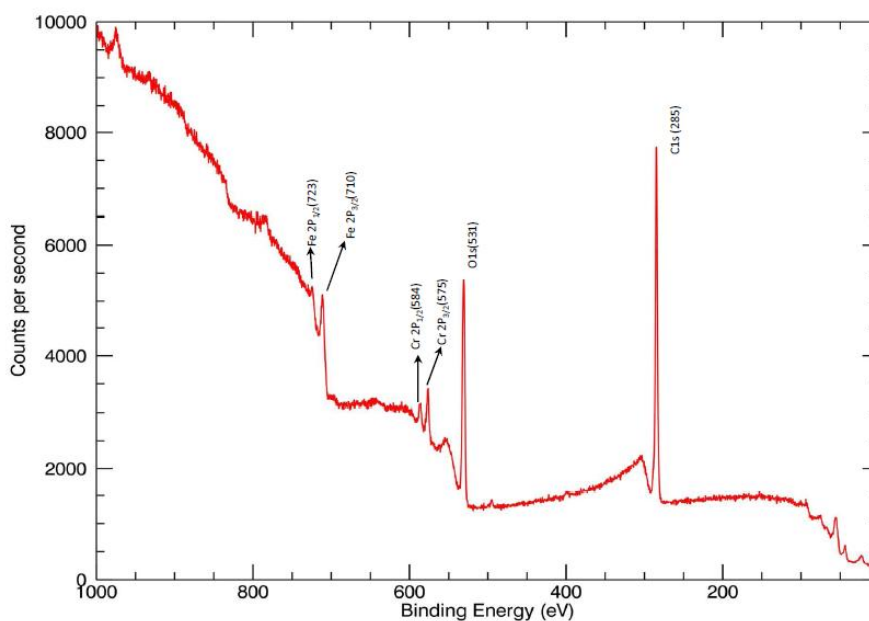
Figure 3. XPS spectra of the corroded area of steel after a potentiostatic polarisation at -1.3 V and a potentiodynamic polarisation in a 1 M sodium chloride solution. (a) survey spectrum (b) Fe_2O_3 and Cr_2O_3 spectra with the relative references.
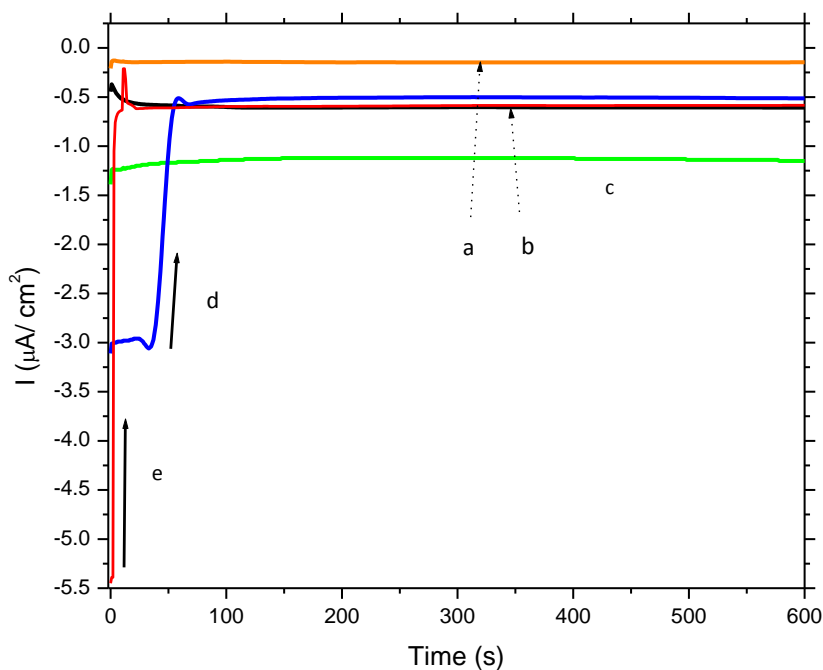

Figure 4. Time dependence of the reduction current of steel using a ca. 200 μm microcapillary in a 1 M sodium chloride solution during the potentiostatic polarisation at five different potentials (a) -1 V, (b) -1.3 V, (c) -1.5 V, (d) -1.7 V and (e) -1.9 V.

The observed results in this work are in good agreement with the results reported by Luo et al. [8], who have studied the synergistic effect of hydrogen and chloride ions on the corrosion performance of 304L stainless steel. They also observed that hydrogen and chloride ions increase the anodic current density and also hydrogen enhances the effect of chloride ions on the pitting potential of steel something which supports our observations.

Variations of the reduction current versus time during the potentiostatic polarisation are shown in Figure 4. The reduction current increases together with the increase in the applied cathodic potential from -1 V to -1.3 V and then to -1.5 V during the cathodic polarisation and can be ascribed to the formation of hydrogen and the produced current at potentials lower than -1.3 V. During the polarisation at -1.7 and -1.9 V the reduction currents show at the beginning higher values, but a rapid decrease is observed after ca. 50 s for -1.7 V and immediately after the beginning of the polarisation for -1.9 V (shown in the figure by arrows). After this decrease the reduction currents show almost stable values between the currents obtained after the first and the second polarisation (at -1 V and -1.3 V). We attribute the observed current decrease at high cathodic potentials to the rapid increase of the charged hydrogen concentration near the tip of the microcapillary which causes the generation of high amounts of gas bubbles and other reduced species. In what follows we show how this current drop effects the impedance spectra of the polarised surface.
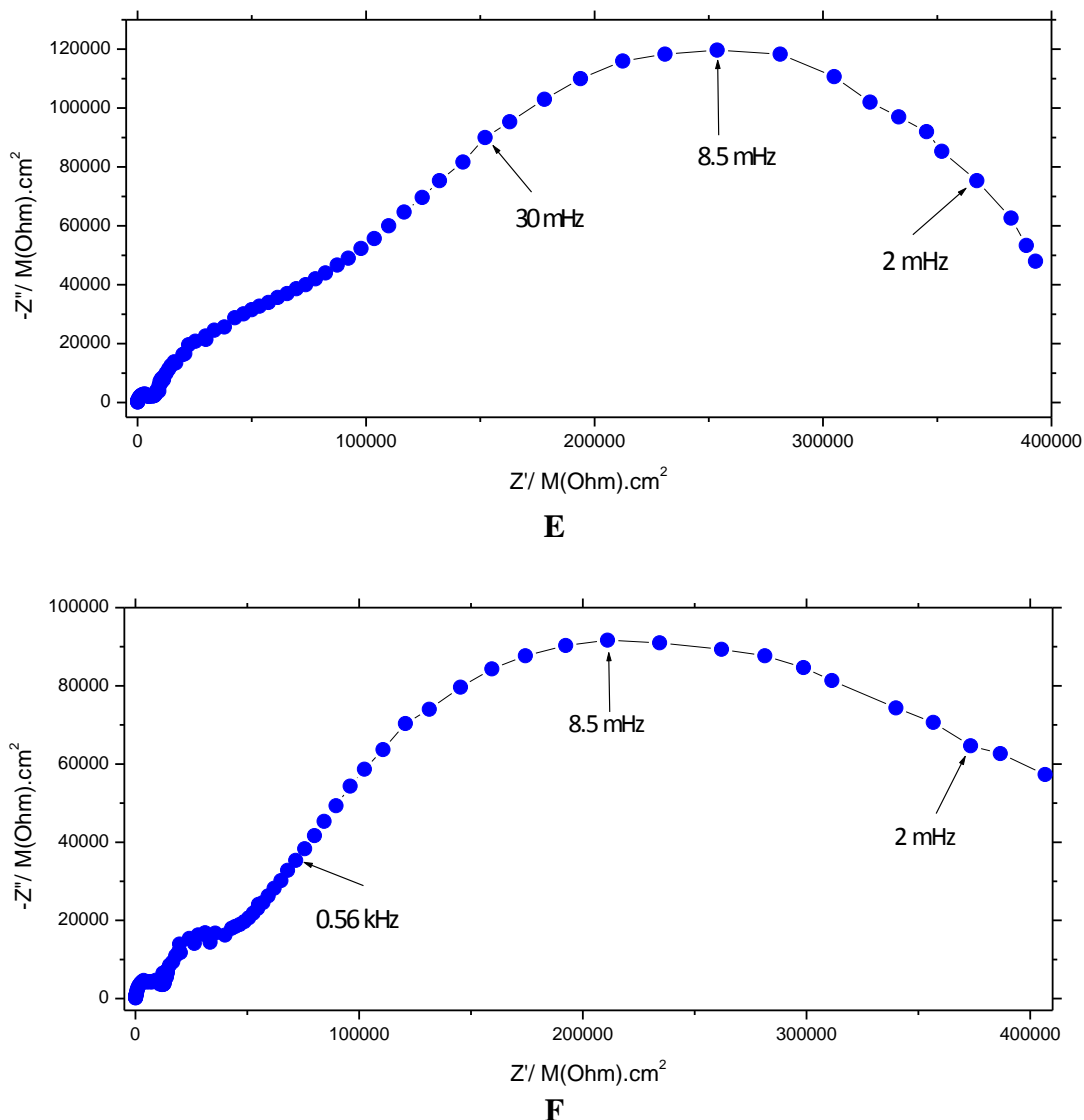
3.2. Local electrochemical impedance spectroscopy (LEIS)

A

B

C

D

E

F
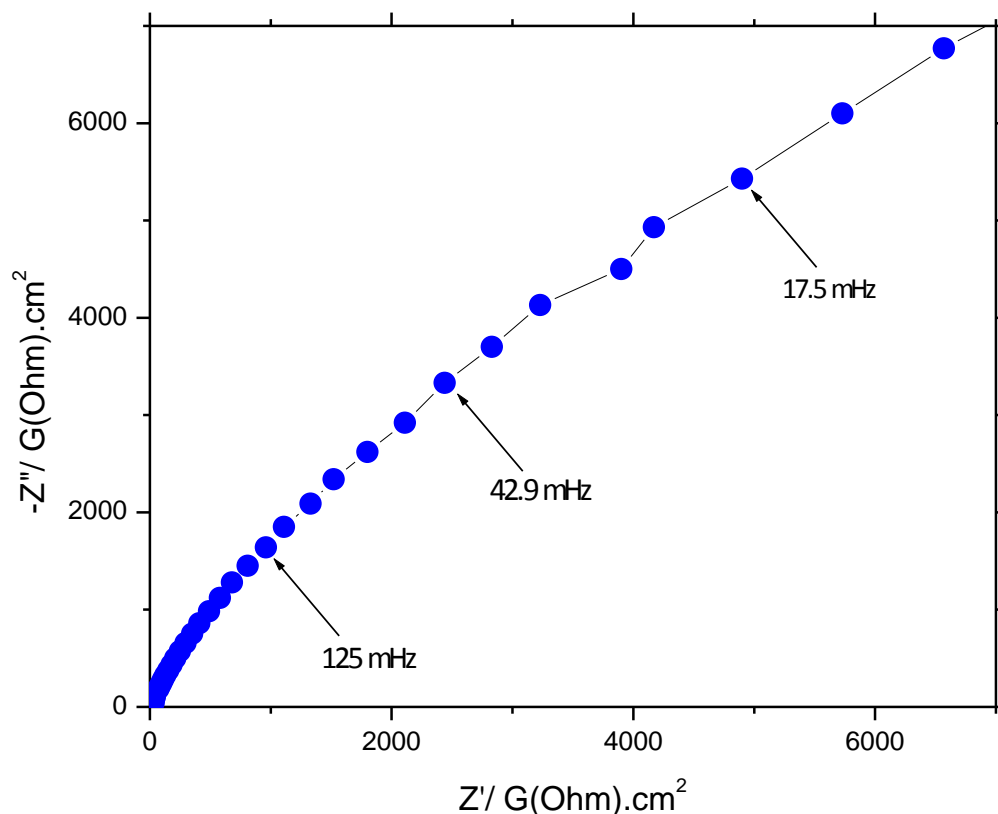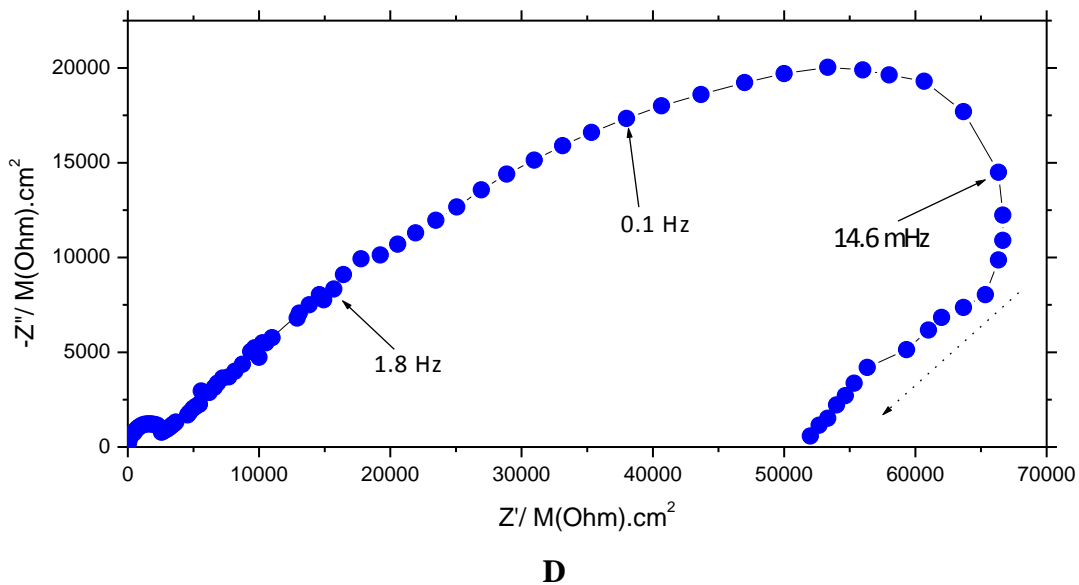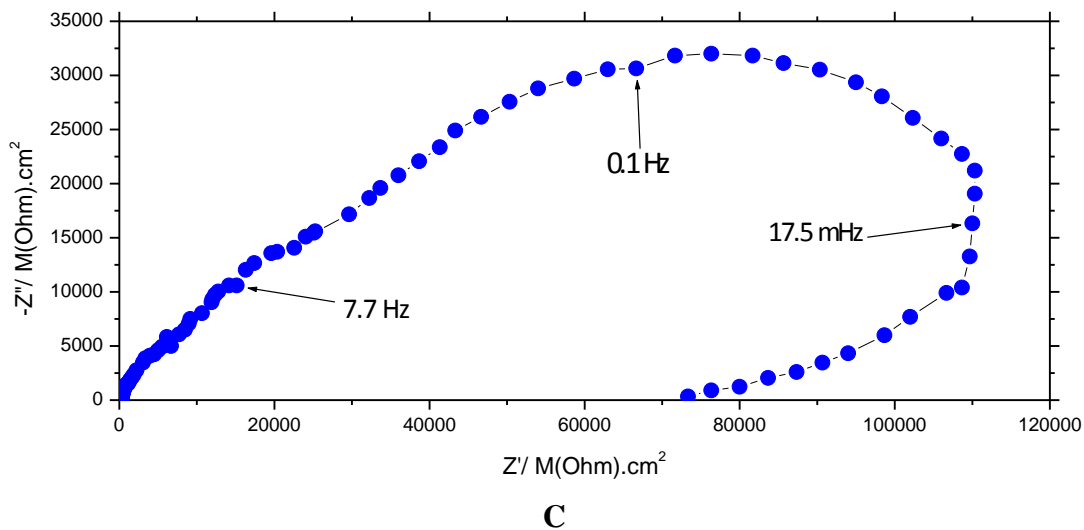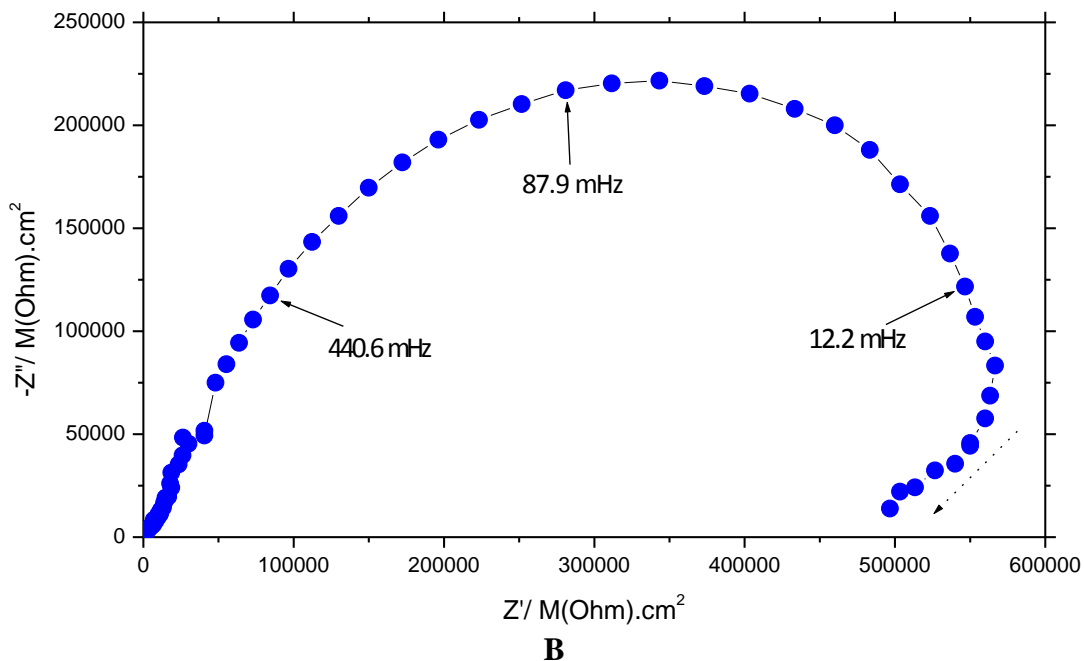
Figure 5. Nyquist graphs obtained locally (a) before and after the cathodic polarisation of steel at five different potentials (b) -1 V, (c) -1.3 V, (d) -1.5 V, (e) -1.7 V and (f) -1.9 V.

Figure 5 shows the Nyquist plots of the steel specimen before and immediately after the cathodic polarisation at respectively -1, -1.3, -1.5, -1.7 and -1.9 V (vs. Ag/AgCl). They were recorded using a microcapillary with the same tip diameter as the measurements described above (ca. 200 μm). The Nyquist graph of the non-polarised sample (a) consists of only one capacitive arc. When applying the cathodic polarisation of -1 V during 600 s, the graph (b) changes to a relaxation impedance (ca. 170×70 M(Ohm).cm^2) with an inductive behaviour at low frequencies (< 12 mHz), which is shown by the dotted arrow. It is attributed to the small ratio of the active surface area in comparison to the passive surface area on the solid surface. The relaxation impedance represents a Faradaic impedance at non-equilibrium potential with a potential-dependent transfer reaction rate. The low frequency inductive behaviour is explained by several other factors such as: instrumental artefacts, adsorbed intermediates or solution soluble intermediates, indirect four-electron reaction or a two-electron reduction oxygen reduction followed by a disproportionation reaction [34].

However, increasing the cathodic potential to -1.3 V decreases the diameter of the semicircle (c) to ca. 35×10 M(Ohm).cm^2 with an inductive loop at low frequencies (< 17 mHz). This reduction in diameter of the Nyquist semicircle after applying a higher cathodic potential is in agreement with the potentiodynamic polarisation graphs in Figure 2. Here changing the cathodic polarisation potential from -1 V to -1.3 V results in a shift of the pitting potential and also the corrosion potential towards more negative potentials and increases the anodic current density and therefore the corrosion resistance decreases. After applying a potential of -1.5 V, the Nyquist graph (d) shows a small semicircle at high frequencies, which in the rest of the graph changes to a larger depressed semicircle. In this case also a low frequency inductive loop is observed. However, the diameter of the Nyquist graph decreases to (ca. 20×6 M(Ohm).cm^2) which once again confirms the lower corrosion resistance of the sample after polarisation at higher cathodic potentials. Finally after the cathodic polarisation the sample at -1.7 and -1.9 V, the diameter of the obtained Nyquist graphs (e, f) increases once again (ca 120×30-35 M(Ohm).cm^2) which implies an increase in the corrosion resistance. These graphs also show a small semicircle at high frequencies, but in spite of the previous Nyquist graphs, they do not show any inductive impedance at low frequencies.

The localised impedance results obtained in this work are interestingly similar with the results which were reported by Oltra and Keddam and also by Sheffer and Vivier [36-38]. These authors have used these spectra to describe the presence of a passive film or an imperfect coating layer with small pinholes. However, the Nyquist graphs of this work are flattened and do not represent regular semicircles and for instance Figure 5 (b and c) contains a straight line at the high frequency end which can be attributed to the diffusional impedance [39]. The roughness of the highly dispersed solid surface has been also reported by Mueller and Urban as a reason of the distortion in the impedance spectra [40].

4. CONCLUSIONS

304L stainless steel was cathodically polarised on a micro scale level and the influence of this polarisation on the surface structure and corrosion resistance of this alloy was investigated. Depending on the conditions of the applied potentiostatic polarisation, the concentration of the generated hydrogen and therefore the adsorbed hydrogen atoms concentration in the electrolyte/ surface interface varies. This directly causes E_{corr}, I_{corr} and also E_{pit} to shift during the anodic dissolution. E_{corr} and E_{pit} decrease continuously while applying more negative potentials. The anodic current density and therefore I_{corr} on the other hand increase when a higher cathodic potential is applied.

When the amount of hydrogen bubbles inside the microcapillary increases (especially during the polarisation at high cathodic potentials) a rapid decrease in the reduction current and moreover an increase in its impedance value is observed which represents the low amount of charged hydrogen. This can be considered as a drawback of the microcapillary technique.

Local electrochemical impedance spectroscopy of the cathodically corroded sample reveals that the corrosion resistance of the steel decreases when the charged hydrogen is introduced into the

surface. The obtained Nyquist graphs however show a different surface behaviour of the sample before and after cathodic polarisation by different applied cathodic potentials.

References

1. W. J. Lee and S. I. Pyun, *Mat. Sci. E*ng., A 279 (2000) 130.
2. H. W. Pickering and R. P. Frankenthal, *J. Electrochem. Soc.*, 119 (1972) 1297.
3. L. J. Qiao, W. Y. Chu and C. M. Hsiao, *Scr. Metall.*, 22 (1988) 627.
4. L. J. Qiao, J. L. Luo and X. Mao, *Corrosion*, 54 (1998) 115.
5. Y. P. Kim, M. Fregonese, H. Mazille, D. Feron and G. Santarini, *Corros. S*ci., 48 (2006) 3945.
6. R. Nishimura, *Mater. Sci. Eng.*, A 25 (1991) 1074.
7. M. Hasegava and M. Osawa, *Corrosion*, 39 (1983) 115.
8. Q. Yang, L. J. Qiao, S. Chiovelli, and J. L. Luo, *Corrosi*on, 54 (1998) 628.
9. H. Yashiro, B. Pound, N. Kumagai and K. Tanno, *Corros. Sci.*, 40 (1998) 781.
10. N. Nishimura, H. Habazaki, A. Kawashima, K. Asami and K. Hashimoto, *Mater. Sci. Eng*., A 134 (1991) 1074.
11. Q. Yang and J. L. Luo, *Electrochim. Acta*, 45 (2000) 3927.
12. Z. Y. Liu, X. G. Li and Y. F. Cheng, *Electrochim. Acta*, 56 (2011) 4167.
13. D. P. Escobar, C. Minambres, L. Duprez, K. Verbeken and M. Verhaege, *Corros. Sci.*, 53 (2011) 3166.
14. Y. Yao, L. J. Qiao and A. A. Volinsky, *Corros. Sci.*, 53 (2011) 2679.
15. H. S. Klapper, J. Goellner and A. Heyn, *Corros. Sci.*, 52 (2010) 1362.
16. Y. F. Cheng and L. Niu, *Electrochem. Comm.*, 9 (2007) 558.
17. M. C. Li and Y. F. Cheng, *Electrochim. Acta*, 52 (2007) 8111.
18. Y. F. Cheng, *J. Mater. Sci.*, 42 (2007) 2701.
19. S. Gudic, J. Radosevic, I. Smoljko and M. Kliskic, *Electrochim. Acta*, 50 (2005) 5624.
20. M. Kliskic, J. Radosevic and S. Gudic, *Electrochim. Acta*, 48 (2003) 4167.
21. K. Genel, M. Demirkol, and M. Urgen, *Int. J. Fat*igue, 24 (2002) 537.
22. P. Rodriguez, F. D. Tichelaar, M. T. M. Koper and A. I. Yanson, *J. Am. Chem. Soc.*, 133 (2011) 17626.
23. M. Sanchez, J. Gamby, H. Perrot, D. Rose and V. Vivier, *Electrochem. Commun*., 12 (2010) 1230.
24. M. Schneider, U. Langklotz, A. Michaelis and B. Arnold, *Surf. Interface Anal.*, 42 (2010) 281.
25. J. Jorcin, H. Krawiec, N. Pebere and V. Vignal, *Electrochim. Acta*, 54 (2009) 5775.
26. H. Krawiec, V. Vignal and R. Akid, *Electrochim. Acta*, 53 (2008) 5252.
27. C. Dong, A. Fu, X. Li, and Y. Cheng, *Electrochim. Acta* 54 (2008) 628.
28. F. Andreatta, M. Lohrengel, H. Terryn and J. Wit, *Electrochim. Acta*, 48 (2003) 3239.
29. T. Hamelmann and M. Lohrengel, *Electrochim. Acta*, 47 (2001) 117.
30. F. Arjmand, and A. Adriaens, *Electrochim. Acta*, 59 (2012) 222.
31. P. V. Mahalakshmi, S. C. Vanithakumari, J. Gopal, U. K. Mudali and B. Raj, *Current Sci*., 101 (2011) 1328.
32. ASTM E 112 – *Standard test methods for determining average grain size*, p. 229-251 (NTU).
33. N. Birbilis, B. N. Padgett and R. G. Buchheit, *Electrochim.* Acta, 50 (2005) 3536.
34. A. M. P. Simoes, M. G. S. Ferreira, B. Rondot and M. da Cunha Belo, *J. Electrochem.* Sco., 137 (1990) 82.

35. P. Schmuki and H. Bohni, *J. Electrochem. Sco*., 139 (1992) 1908.
36. R. Oltra and M. Keddam, *Electrochim. Acta*, 35 (1990) 1619.
37. R. Oltra and M. Keddam, *Corros. Sci.*, 28 (1988) 1.
38. M. Sheffer, V. Vivier and D. Mandler, *Electrochem. Comm*., 9 (2007) 2827.
39. T. Jacobsen and K. West, *Electrochim. Acta*, 40 (1995) 255.
40. T. Mueller and P. M. Urban, *J. Power Sources*, 75 (1998) 139.